

Supporting Information for

Correlating Structural and Functional Heterogeneity of Immobilized Enzymes

Daniel F. Kienle, Rebecca M. Falatach, Joel L. Kaar, Daniel K. Schwartz**

Department of Chemical and Biological Engineering, University of Colorado, Boulder, CO 80309

*Corresponding Authors

Joel L. Kaar: joel.kaar@colorado.edu

Daniel K. Schwartz: daniel.schwartz@colorado.edu

Table of Contents

1. Detailed Image Analysis	2
Figure S1.....	4
2. Sensitivity to Blink Tolerance, Intensity Cutoff, and Bleach-Time Cutoff	5
Figure S2.....	6
Figure S3.....	7
Figure S4.....	8
3. Modeling Enzyme Conformation	8
4. Modeling Substrate Binding	11
5. Derivation of Equation S5	13
6. Estimation of the Fraction Falsely Identified Binding Events	15
7. Lower Bound Estimate of Substrate Binding Rate for FMN on Fully Active Non-Specifically Tethered NfsB	16
8. Supplemental Figures	17
Figure S5.....	17
Figure S6.....	18
Figure S7.....	19
Figure S8.....	20
Figure S9.....	21
Figure S10.....	22
Figure S12.....	24
Figure S13.....	25
Figure S14.....	26
9. References	26

1. Detailed Image Analysis

All image analysis was performed using Matlab-based software written in house. For both binding and conformation studies, the two imaging channels were aligned using a non-uniform pixel displacement field. The image used to determine the displacement field consisted of time-average image of all frames from one or more of the videos or a scratched slide illuminated with white light and imaged using the experimental set up. The latter was necessary for binding experiments where objects colocalized between channels were the minority. Fluorescent objects in each channel and excitation were identified using a user-defined background removal and thresholding procedure. The positions of the fluorescent molecules were quantified by fitting a linearized circular Gaussian to the background subtracted intensities of the pixels encompassing each object, while the intensity was taken as the sum of these background subtracted pixel intensities.

The objects identified in each channel during the Donor (532nm) excitation of the ALEX-SM-FRET experiments were colocalized within a radius of two pixels (440 nm). These objects were then colocalized with the objects detected during the red excitation using the same radius. All objects that were not detected during both excitations were discarded as mislabeled. At this point, the acceptor-excited data was discarded and all further analysis was performed on the donor excitation results. Trajectories were identified by colocalizing the objects in subsequent frames within a radius of 2 pixels, which accounts for localization error.

For binding experiments, the emission from the Alexafluor 647 labeled NfsB was too weak to consistently identify objects in individual frames. Instead, an average z-projection of the red channel was used to identify and locate the enzymes. The substrates identified in the blue channel from each frame were then colocalized with the known enzyme positions. Details on the method for channel

alignment, object identification, intensity quantification, and colocalization of objects in either channel can be found elsewhere.¹ Here, the uncertainty in object intensity was calculated as $\delta = \sqrt{2(N - B)/F}$ where N is the object intensity counts, B is the baseline count added to the camera signal, F is the camera-specific count-to-photon conversion factor, and the $\sqrt{2}$ factor is the additional noise multiplier that results from the electron multiplying process of the EMCCD camera. This uncertainty is equivalent to shot noise multiplied by $\sqrt{2}$.

To prevent noise from being misidentified as objects, any detected substrate or dual labeled enzyme that did not last more than two frames (200 ms for substrates, 400 ms for NfsB_{FRET} molecules) was removed from the data. The data was also filtered to remove potential aggregates. To do this, both the trajectory duration (*i.e.* time to photobleach) and trajectory median intensity in each channel were assigned a cutoff at the parametric 95th percentile, above which trajectories were discarded. To reduce the effect of very large outliers that are occasionally measured, the cutoff for each intensity was estimated as $2 * \sigma \approx 2 * 1.4826 * MAD(I)$ where $MAD(I)$ is the mean absolute deviation of the set of trajectory median intensities, I . The trajectory duration cutoff was defined as the 95th percentile of the best-fit exponential distribution. No aggregate removal procedure was applied to the binding data, as aggregates were not expected to significantly affect binding results, which have no sensitivity to object intensity or trajectory duration.

Premature loss of a trajectory sometimes occurs during tracking conformation data due to the signal dipping below the object detection threshold. This can be a result of shot noise, photo-blinking, or mid-frame FRET state transitions causing a reduced intensity in both channels. To overcome this effect, trajectories that were in the same location but separated by a short time were linked, and the missing entries in the trajectory data were assigned values. The position data for the frames where the object was not detected were set to the average of all other positions of the trajectory, and the intensity data was calculated from the raw image data of the corresponding frame, using the same

method as was used to quantify the intensities of the detected objects. This procedure was performed after applying the excitation colocalization and minimum residence time cutoff, which prevents noise from artificially extending trajectories. The allowable duration of reduced intensity (hereon referred to as the blink tolerance) was set to five frames (1 second). In general, increases in the blink tolerance between 0 and 10 frames increased the exponentiality of the distribution of trajectory durations as shown in **Figure S1**, indicating that the added blink tolerance allowed objects to be more consistently tracked until photobleaching, which is theoretically expected to be exponential.

Finally, objects that were initially detected at a time greater than one blink tolerance from the start of the movie were discarded to prevent the adsorption of fluorescent contaminants (including mobile, labeled enzyme) from affecting the results.

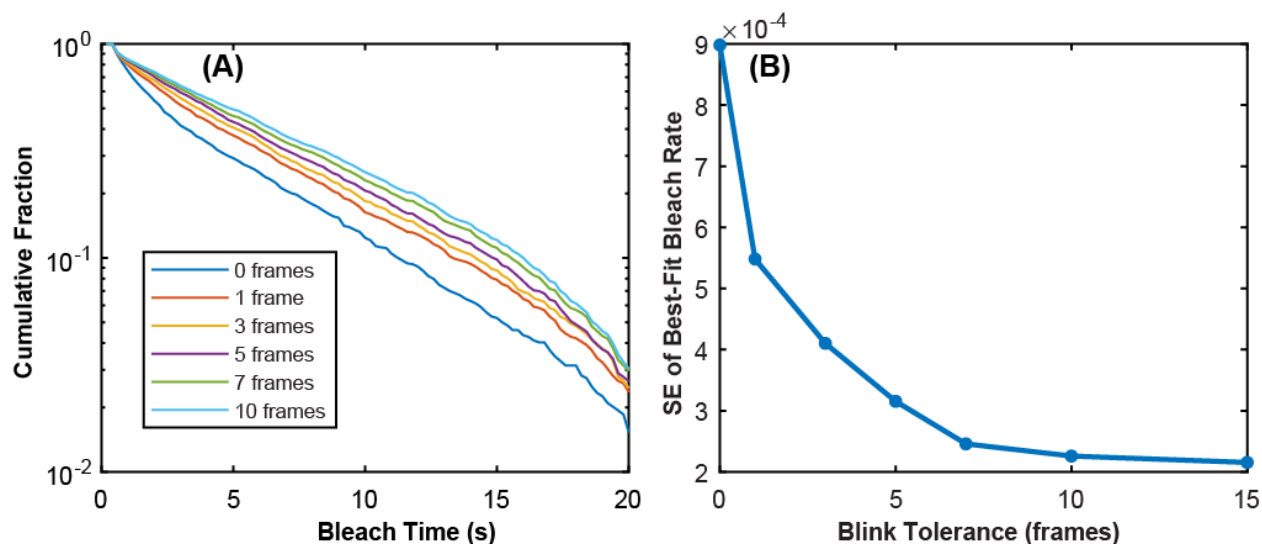


Figure S1 (A) Semi-log plot showing the complimentary cumulative distribution of the bleach times (duration that an object is observed prior to photobleaching) for non-specifically tethered NfsB analyze with varying blink tolerances. The distribution becomes increasingly exponential (the theoretically expected distribution of bleach times) as longer blinks are tolerated, indicating that fewer trajectories are being lost prematurely. (B) A plot of the standard error of the rate parameter for the best-fit exponential distribution for each blink tolerance, averaged for all 9 conditions (i.e., immobilization methods and urea concentrations). This is used as a quantitative measure of the exponentiality of each distribution in (A), and demonstrates that the bleach times are continuously more exponential as the blink tolerance is increased. This indicates that trajectories are not being prematurely lost. A conservative blink tolerance of 5 frames was selected to prevent trajectories from being predominantly composed of low intensity objects.

2. Sensitivity to Blink Tolerance, Intensity Cutoff, and Duration Cutoff

A sensitivity analysis was performed by varying median intensity cutoff, duration (residence time) cutoff, and blink tolerance. Each variable was varied one-at-a-time from the base values (i.e., the values used in the manuscript). Specifically the median intensity cutoff was defined as 1σ , 2σ and 3σ where $\sigma \approx 1.4826 * MAD(I)$; the residence time cutoff was defined at 68th, 95th, and 99.7th percentile of the best fit exponential distribution; and the blink tolerance was defined as 2, 5, and 8 frames, where the middle value for parameters was the base value. The results were used to calculate the folded fraction and average number of transitions for each condition, which are plotted in **Figure S2** and **Figure S3**, respectively. For the most part the folded fraction shows a weak sensitivity to all 3 parameters, and the reported trend is maintained at all tested parameter sets. The variation in the transition rates with changes to the parameters is more significant. However, the observed trend is similar with all parameter sets. The analysis of the substrate binding rate on folded enzymes, $\bar{\lambda}_{folded}$, were also carried out using the results of the sensitivity analysis, and the models described in section 4. These are shown in **Figures S4**. While the values determined using different parameter sets are nominally different, the main conclusions can still be drawn from all of the data sets. Specifically, the value of $\bar{\lambda}_{folded}$ significantly increases from adsorbed NfsB to tethered NfsB, and from nonspecifically tethered NfsB to site-specifically tethered NfsB in all cases. Thus, variation in these selected parameters does not alter the important finding reported in the manuscript.

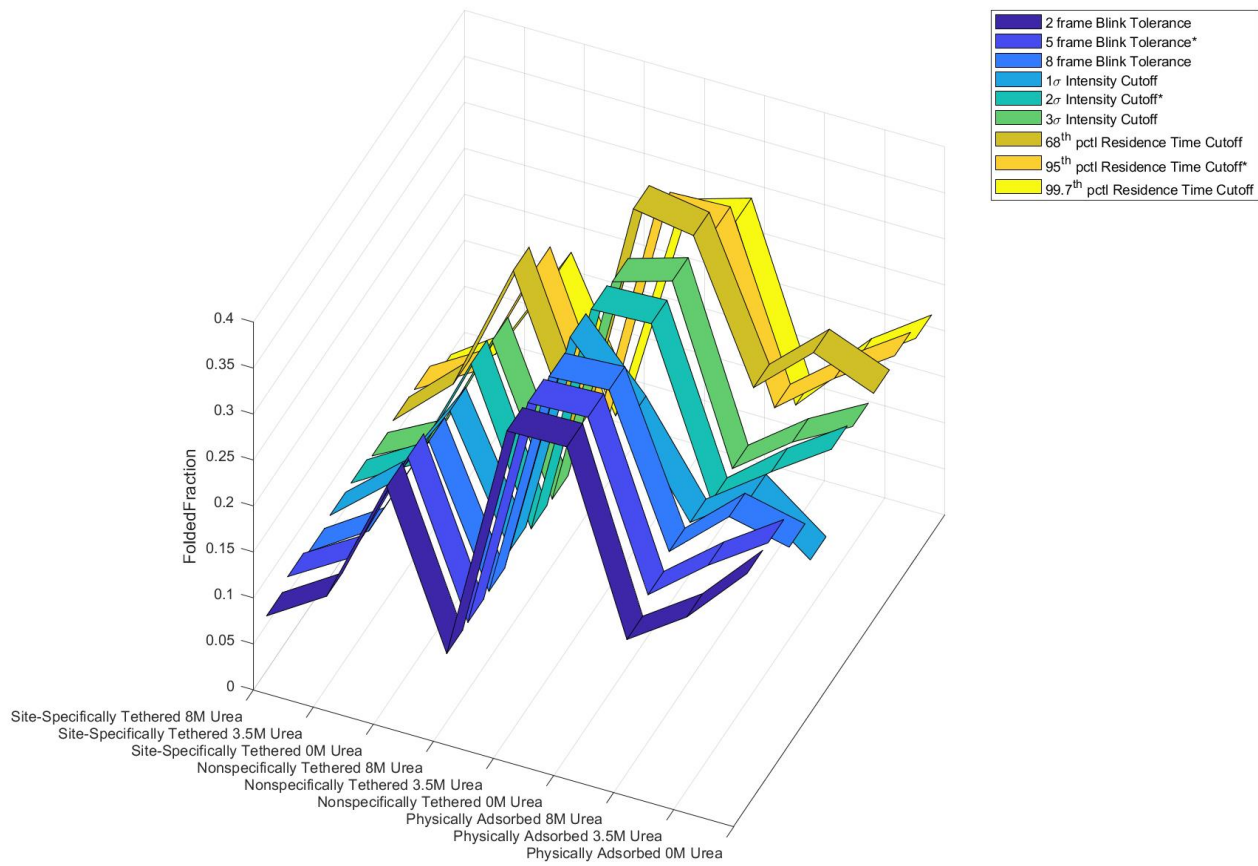


Figure S2 Ribbon plots showing the folding fraction of the 9 conditions (x-axis) determined from data analyzed using the indicated blink tolerance, intensity cutoff, or residence time cutoff with the other two parameters set to the values used to produce the results reported in the manuscript (indicated in the legend with an asterisk).

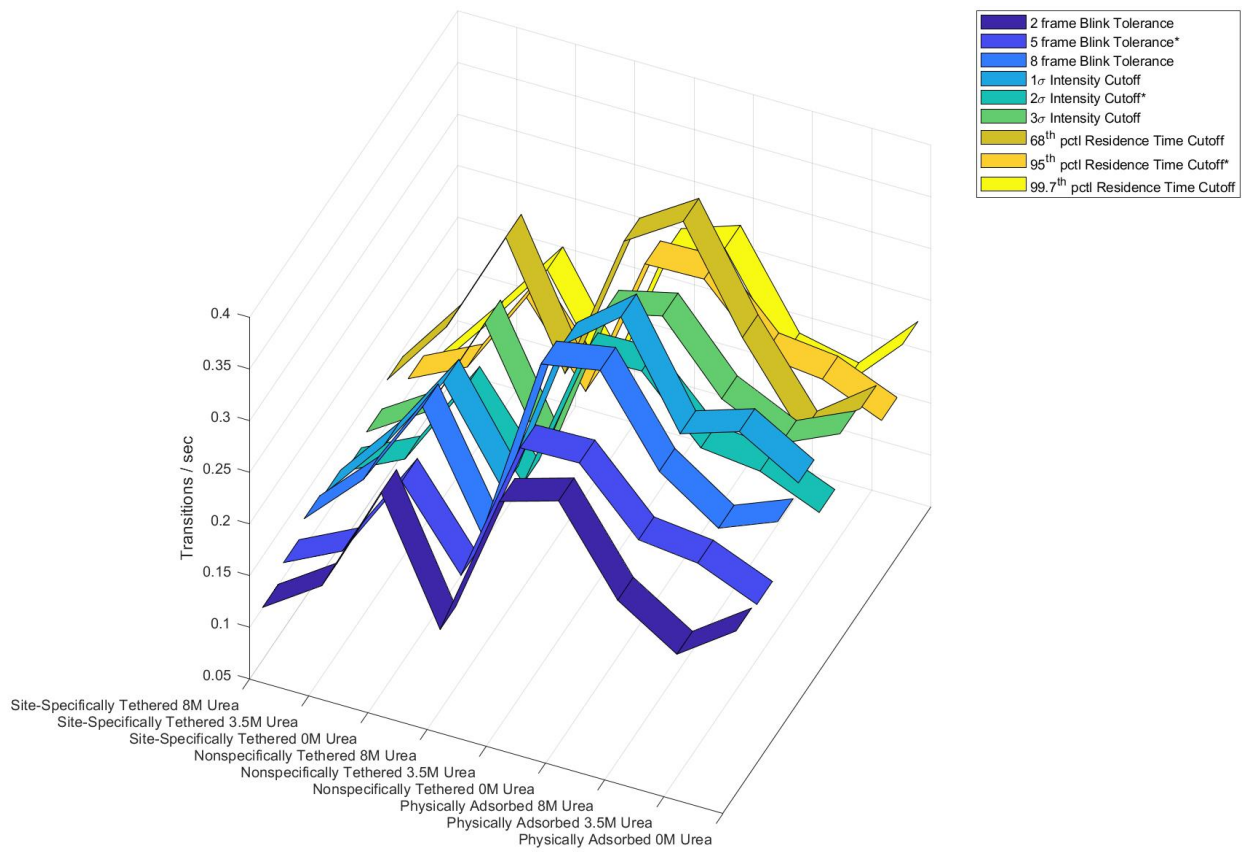


Figure S3 Ribbon plots showing the average counted transition/second of the 9 conditions (x-axis) determined from data analyzed using the indicated blink tolerance, intensity cutoff, or residence time cutoff with the other two parameters set to the values used to produce the results reported in the manuscript (indicated in the legend with an asterisk).

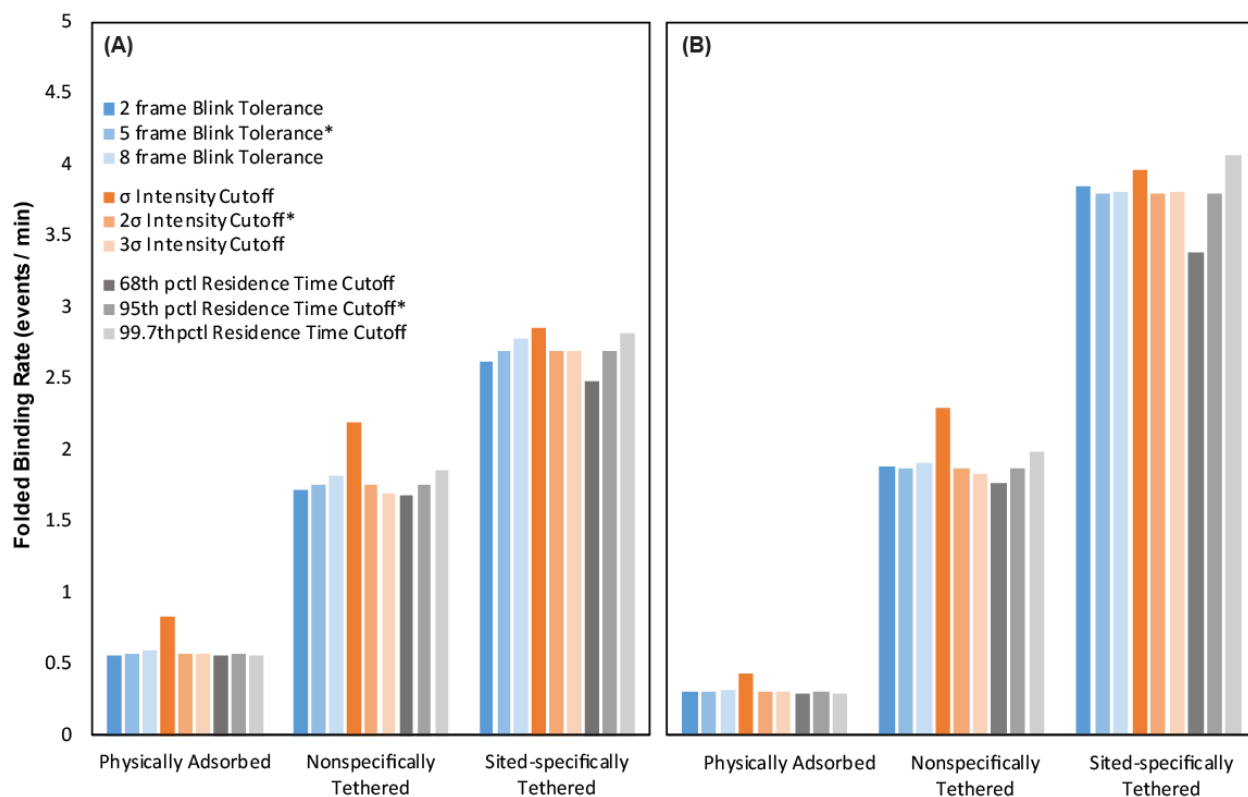


Figure S4 Bar plots showing the folded binding rate ($\bar{\lambda}$) of (A) LF and (B) FMN determined from data analyzed using the indicated blink tolerance, intensity cutoff, or residence time cutoff with the other two parameters set to the values used to produce the results reported in the manuscript (indicated in the legend with an asterisk).

3. Modeling Enzyme Conformation

The folding states of the enzymes were modeled using a 3-state Markov chain model, in which enzymes can take on an unfolded, folded or photobleached state (it was important to account for photobleaching because the acceptor dye bleached on a similar time scale to the enzyme folding transitions). The transition probability matrix takes the form,

$$TR = \begin{pmatrix} 1 - p_f - p_b & p_f & p_b \\ p_u & 1 - p_u - p_b & p_b \\ 0 & 0 & 1 \end{pmatrix} \quad (S1),$$

where p_f , p_u , and p_b are the probabilities that a molecule will fold, unfold or bleach between two consecutive frames. The value of p_b was independently determined by fitting the distribution of times before the first fluorescent label bleaches to an exponential distribution. The bleaching rate was treated as identical for both folded and unfolded molecules, which is reasonable because both the acceptor and donor label were directly excited throughout the video, and the directly excited acceptor dye bleached much faster than donor-excited acceptor dye for both high and low FRET molecules. The values for p_f and p_u were estimated by maximizing the likelihood function,

$$LF(S|p_f, p_u) = \prod_k [\prod_{i=1} TR(S_{i-1,k}, S_{i,k} | p_f, p_u)] \quad (S2),$$

where $\{S_{1,k} \dots S_{n,k}\}$ is the sequence of observed folding states for the k th trajectory. The maximum likelihood estimate can be defined explicitly for this as

$$\hat{p}_u = \frac{N_{fu}(1-p_b)}{N_{ff}+N_{fu}} \quad (S3)$$

and

$$\hat{p}_f = \frac{N_{uf}(1-p_b)}{N_{uu}+N_{uf}} \quad (S4),$$

where N_{uf} , N_{uu} , N_{fu} , N_{ff} , and N_b are the total number times an object folds, remains unfolded, unfolds, or remains folded, respectively, throughout the population. This homogeneous estimate has been used by us previously.²

The simplest form of this model assumes that the folding kinetic are first order and that molecules exhibit homogeneous folding kinetics. The latter assumption is not physically realistic given the heterogeneous environment that the enzymes will experience on the surface. Markov chain

mixtures were employed to account for possible heterogeneity in the enzyme population, where the definition of TR varies between molecules, while remaining constant with time. Specifically, a mixture model of several discrete populations with distinct transition probabilities, and an over-disperse Markov chain model where p_f and p_u vary throughout the population and follow independent beta distributions (chosen for the diversity of the distribution shape and because it is appropriately double bounded). The maximum likelihood estimates could not be defined explicitly for either of these more complex models, so the parameters were estimated using numeric optimization of the likelihood functions. For the discrete TR model, the likelihood was a simple extension of **Eq S2**,

$$LF(S|f, p_f, p_u) = \prod_k [\sum_j f_j * \prod_{i=2} TR_j(S_{i-1,k}, S_{i,k} | p_{f,j}, p_{u,j})] \quad (S5),$$

where f_j is the fraction of the enzyme population that exhibits the i th transition matrix and transition probabilities. The log of LF was maximized by varying the values of f , p_f , and p_u , which make up 5 parameters for a 2-population model.

The likelihood function for the model with Beta-distributed transition probabilities is given by

$$LF(S|a_f, b_f, a_u, b_u) = \prod_k \left[\frac{B(a_f + N_{uf,k}, b_f + N_{uu,k}) B(a_u + N_{fu,k}, b_u + N_{ff,k})}{B(a_f, b_f) B(a_u, b_u)} p_b^{N_{b,k}} (1 - p_b)^{N_{uu,k} + N_{uf,k} + N_{ff,k} + N_{fu,k}} \right] \quad (S6),$$

where B is the beta function. The model is parameterized by a_f , b_f , a_u , and b_u , which are the parameters defining the beta distribution of p_f and p_u , respectively. These values were estimated by maximizing the log of the likelihood function given by **Eq S6**. The derivation of **Eq S6** is given in section 5. Once the average maximum-likelihood estimates of the transition probabilities, \hat{p}_u and \hat{p}_f , were determined, the average folding and unfolding rate constant could be estimated as $k_f = -\log(1 - \hat{p}_f) / (\tau - \tau p_b)$ and $k_u = -\log(1 - \hat{p}_u) / (\tau - \tau p_b)$ where τ is the frame acquisition

time. For the beta-distributed transition probabilities, this translated to average rate constants of $k_f = -(\psi(b_f) - \psi(a_f + b_f)) / \tau$ and $k_u = -(\psi(b_u) - \psi(a_u + b_u)) / \tau$, respectively, where ψ is the digamma function.

4. Modeling Substrate Binding

As described in the manuscript, to account for enzyme conformation, the average binding rate, λ , was defined as $\lambda = \lambda_0 * x$, returning a binding rate distribution of

$$P_{bind}(k|\lambda_0) = \int_0^1 \frac{(\lambda_0 * x)^k \exp(-\lambda_0 * x)}{k!} * P_{fold}(x) dx \quad (S7)$$

where λ_0 represents the unperturbed binding rate of a fully functional and active enzyme, k is the number of observed binding events, and x is the fraction of time an enzyme spends folded which is distributed by the probability density function, P_{fold} . Additional contributions were considered by redefining λ as $\lambda = \lambda_0 * x * y$. Applying this to **Eq. S8** gives a binding rate distribution of

$$P_{bind}(k) = \int_0^1 \int_0^1 \frac{(\lambda_0 * x * y)^k \exp(-\lambda_0 * x * y)}{k!} * P_{fold}(x) * P_{active}(y) dy dx \quad (S8),$$

where y is the fraction of full activity of an enzyme whose folded activity, λ_0 , is reduced by a system property that is independent of the folding state and P_{active} is the probability distribution of y . This can be thought of as an additional reduction in the activity of folded enzymes that would otherwise be fully active.

This approach was used to introduce one additional fitting parameter, p_{active} , which is the fraction of time a folded enzyme is also fully active. This was applied to **Eq. S9** by defining $P_{active}(y|p_{active})$ as a Bernoulli distribution, yielding the zero-inflated Poisson mixture,

$$P_{bind}(k|\lambda_0, p_{active}) = p_{active} \int_0^1 \frac{(\lambda_0 * x)^k \exp(-\lambda_0 * x)}{k!} * P_{fold}(x) dx \quad (S9).$$

The distribution P_{fold} was estimated for each of the conformation state models described above by defining a probability mass function based on simulations of 50,000 trajectories. The simulations were defined by the conformation models and maximum likelihood estimates described in the previous section, except that the photobleaching probability, p_b , was set to zero, the other probabilities defined in **Eq. S1** were accordingly renormalized, and the duration of each trajectory was equal to the movie length used for binding experiments of one minute. For the Markov chain mixture models, prior to simulating the state sequence, each trajectory was assigned values for p_f and p_u , as well as an initial state of either folded or unfolded. The transition probabilities for each trajectory of the models that use a mixture of discrete transition matrices were assigned by direct sampling according to the population fractions, f in **Eq. S5**. For the Markov chain mixture with Beta-distributed transition probabilities, the transition probabilities for each trajectory were randomly sampled from the best-fit beta distribution using the built-in Matlab function *betarnd*. After the transition matrix was defined, the initial state was randomly selected according to the probability of occupying either state at equilibrium, P_{eq} . The equilibrium probability was determined by

$$P_{eq} = [0 \quad 1] * TR^\infty = \frac{1}{p_f + p_u} * [p_u \quad p_f] \quad (S10).$$

Maximum likelihood fitting was used to estimate the unperturbed binding rate, λ_0 , and p_{active} where applicable. The likelihood function was simply defined by $LF = \prod_i P_{bind}(k_i)$, where k_i is the number of binding events observed on the i th enzyme and P_{bind} was defined by either **Eq. S8** or **S10**.

5. Derivation of Equation S5

The likelihood function for the Markov-chain with Beta-distributed transition probabilities is given by

$$LF(S|a_f, b_f, a_u, b_u) = \prod_k \left[\int_0^{1-p_b} \int_0^{1-p_b} P_f(p_f|a_f, b_f) P_u(p_u|a_u, b_u) \prod_{i=2}^n TR(S_{i-1,k}, S_{i,k}|p_f, p_u) dp_f dp_u \right] \quad (\text{S11}),$$

where P_f and P_u are the beta distributions of the folding and unfolding transition probabilities and are rescaled to be defined on the interval $(0, 1 - p_b)$ which encompasses all values that p can take. Written out, these take the form

$$P_\beta(p|a, b) = \frac{\left(\frac{p}{1-p_b}\right)^{a-1} \left(1 - \frac{p}{1-p_b}\right)^{b-1}}{B(a, b)} \quad (\text{S12}).$$

By evaluating the product around the transition matrix and considering the likelihood of a single trajectory, k , **Eq. S11** becomes

$$LF_k = \int_0^{1-p_b} \int_0^{1-p_b} P_f(p_f|a_f, b_f) P_u(p_u|a_u, b_u) p_b^{N_{b,k}} p_f^{N_{uf,k}} (1 - p_b - p_f)^{N_{uu,k}} p_u^{N_{fu,k}} (1 - p_b - p_u)^{N_{ff,k}} dp_f dp_u \quad (\text{S13}).$$

The double integral can be separated into the product of two independent integrals, giving

$$LF_k = p_b^{N_{b,k}} \left[\int_0^{1-p_b} P_f(p_f | a_f, b_f) p_f^{N_{uf,k}} (1 - p_b - p_f)^{N_{uu,k}} dp_f \right] \\ \times \left[\int_0^{1-p_b} P_u(p_u | a_u, b_u) p_u^{N_{fu,k}} (1 - p_b - p_u)^{N_{ff,k}} dp_u \right] \quad (S14)$$

These two integral are treated identically from this point on, so we will continue only with the integral with respect to p_f , referred to as

$$I_f = \int_0^{1-p_b} P_f(p_f | a_f, b_f) p_f^{N_{uf,k}} (1 - p_b - p_f)^{N_{uu,k}} dp_f \quad (S15).$$

Substituting **Eq. S12** into **Eq. S15** for P_f returns

$$I_f = \int_0^{1-p_b} \frac{\left(\frac{p_f}{1-p_b}\right)^{a_f-1} \left(1 - \frac{p_f}{1-p_b}\right)^{b_f-1} p_f^{N_{uf,k}} (1-p_b-p_f)^{N_{uu,k}}}{B(a_f, b_f)} dp_f \quad (S16).$$

From here, we divide out $(1 - p_b)$ such that $(1 - p_b)$ has the same degree in the base of each exponential term, giving

$$I_f = \frac{(1-p_b)^{N_{uf,k}+N_{uu,k}}}{B(a_f, b_f)} \int_0^{1-p_b} \left(\frac{p_f}{1-p_b}\right)^{a_f-1} \left(1 - \frac{p_f}{1-p_b}\right)^{b_f-1} \left(\frac{p_f}{1-p_b}\right)^{N_{uf,k}} \left(1 - \frac{p_f}{1-p_b}\right)^{N_{uu,k}} dp_f \quad (\text{S17}).$$

These can then be multiplied to

$$I_f = \frac{(1-p_b)^{N_{uf,k}+N_{uu,k}}}{B(a_f, b_f)} \int_0^{1-p_b} \left(\frac{p_f}{1-p_b}\right)^{N_{uf,k}+a_f-1} \left(1 - \frac{p_f}{1-p_b}\right)^{N_{uu,k}+b_f-1} dp_f \quad (\text{S18}).$$

By rearranging **Eq. S12**, we can see that the integrand of **Eq. S18** is equal to a beta distribution multiplied by its normalizing constant, $P_\beta B$, which is substituted into **Eq. S18** such that

$$I_f = \frac{B(a_f+N_{uf,k}, b_f+N_{uu,k})(1-p_b)^{N_{uf,k}+N_{uu,k}}}{B(a_f, b_f)} \int_0^{1-p_b} P_\beta(p_f | a_f+N_{uf,k}, b_f+N_{uu,k}) dp_f \quad (\text{S19}).$$

At this point, the integral can be evaluated to one, leaving the coefficient. Substituting this and the p_u analog back into **Eq. S14** returns the final likelihood function for a single trajectory,

$$LF_k = \frac{B(a_f+N_{uf,k}, b_f+N_{uu,k})B(a_u+N_{fu,k}, b_u+N_{ff,k})}{B(a_f, b_f)B(a_u, b_u)} p_b^{N_{b,k}} (1-p_b)^{N_{uu,k}+N_{uf,k}+N_{ff,k}+N_{fu,k}} \quad (\text{S20})$$

6. Estimation of the Fraction of Falsely Identified Binding Events

During SM-TIRFCM measurement, substrate adsorption to the surface within the co-localization radius of an enzyme can occasionally be mistaken for active-site binding. To estimate the fraction of binding events that were falsely interpreted adsorption events, we first determined the rate of surface adsorption events (λ_{ads}) by counting the number of non-co-localized substrate molecule adsorption events per frame. We then estimated the fraction of falsely identified binding events (P_{false}) as

$$P_{false} = \frac{\lambda_{ads}N_{enzyme}}{\lambda_{bind}N_{frame}} \quad (S21)$$

where N_{enzyme} is the total number of pixels that were colocalized with an enzyme, and λ_{bind} is the average substrate binding rate (as shown in Figure 5A) and N_{frame} is the total number of pixels in the frame. The results for each immobilization method and enzyme are shown in Table S1. As can be seen, LF had a much higher affinity for the surrounding surface than FMN. Nonetheless, the uncertainties of the mean binding rates, folded binding rates, and $\bar{\lambda}_{folded}$ were greater than $\bar{\lambda}_{folded} * P_{false}$ except in the case of physically adsorbed enzymes where the binding rate was very low. In this case, the bottom error bars were adjusted to reflect the uncertainty due to P_{false} , which would only serve to reduce the average binding rates. These values represent the upper bound estimate, as the calculation of P_{false} does not account for unlabeled NfsB, which exists on the surface, and would inflate the adsorption rate.

Table 1 Values of the estimated fraction of falsely identified binding event due to surface adsorption for each of the substrates and immobilization methods.

	P_{false} FMN Binding	P_{false} LF Binding
Physically Adsorbed	0.20	0.18
Non-specifically Tethered	0.03	0.11
Site-specifically Tethered	0.03	0.10

7. Lower Bound Estimate of Substrate Binding Rate for FMN on Fully Active Non-Specifically Tethered NfsB

The average binding rate of fully active enzymes must be greater than 9 events/min such that all observed binding rates can be explained by either Poisson variance (if greater than the fully active binding rate) or reduced activity (if lower than the fully active binding rate). For this distribution, 8.5 events/min was determined as the minimum value for which the maximum observed binding rate of 18 events/min (which is, most likely, still only partially active) was statistically feasible and would occur with the same probability shown in Figure 6A (0.001).

8. Supplemental Figures

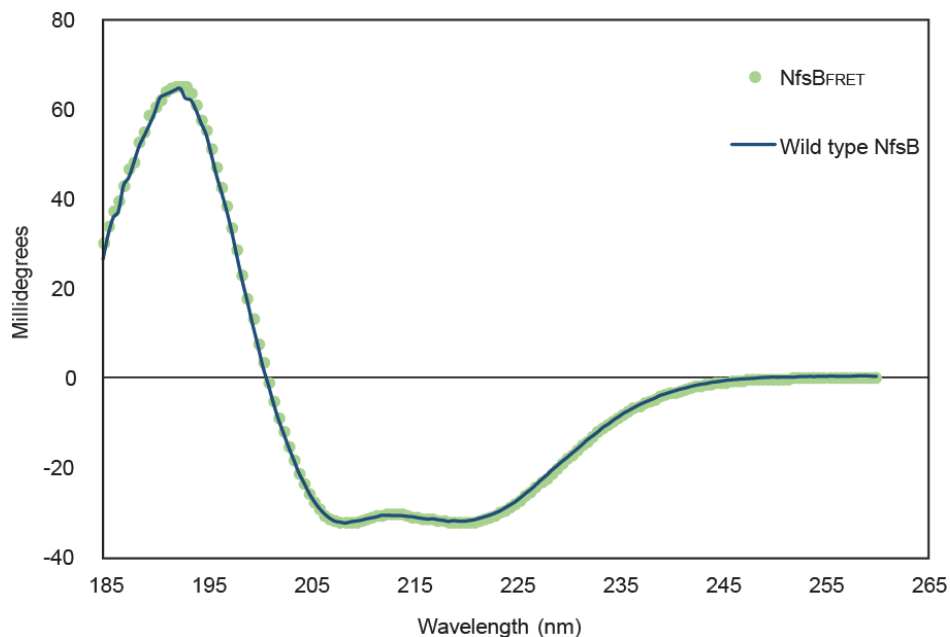


Figure S5 Circular dichroism spectrum of unlabeled NfsB_{FRET} (green circles) mutant and wild-type NfsB (blue line), demonstrating that the structure of NfsB in solution was unaffected by the mutations. The spectra are averaged from three successive scans between 185-260 nm in 0.5 nm increments and an integration time of 0.5 s per increment.

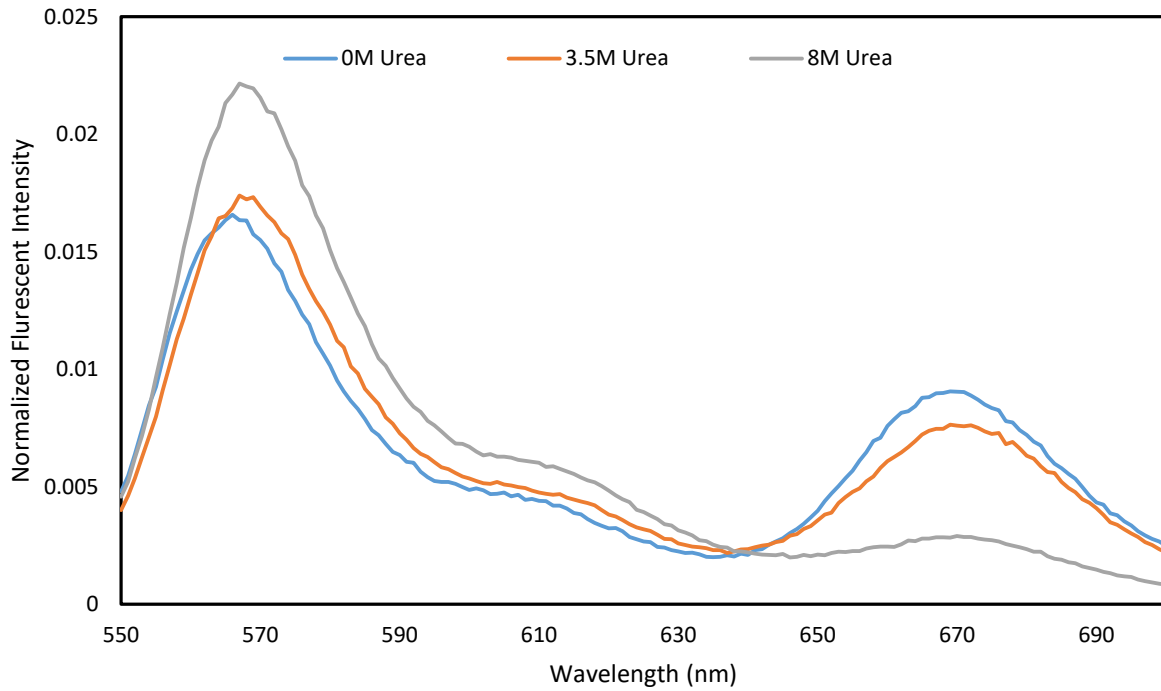


Figure S6 Normalized fluorescent emission of 0.005 μM FRET-labeled NfsB in buffer solutions containing different concentrations of urea. The measurements were taken using an excitation of 532 nm. Estimated FRET efficiencies for each curve were 0.371, 0.317, and 0.12 for NfsB in 0 M, 3.5 M, and 8M urea, respectively, demonstrating that the FRET-labeled NfsB unfolds in urea. These estimates were calculated as $I_A/(I_A + I_D)$ where I_A is the area under each curve from 565nm to 605nm and I_D is the area under each curve from 665nm to 705nm, corresponding to the filtered light detected in each imaging channel during single molecule imaging.

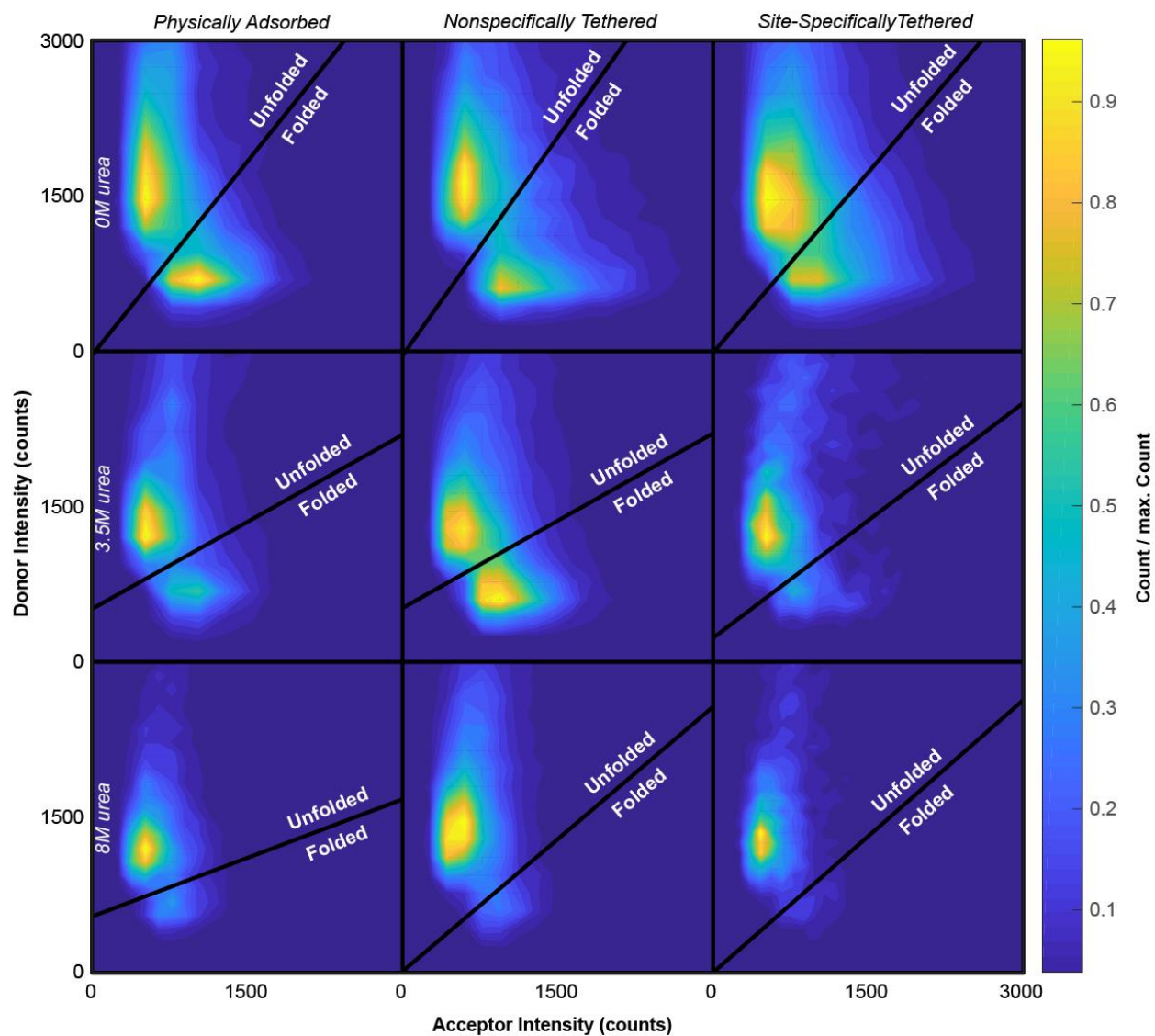


Figure S5 Heat map representations of binned acceptor and donor intensities of immobilized NfsB. All maps shows two discrete population peaks corresponding to folded and unfolded populations, where the black line is used to divide the two populations and assign either a folded or an unfolded state to each observation. From left to right, the plot correspond to physically adsorbed, nonspecifically tethered and site-specifically tethered NfsB, while from top to bottom the figure correspond to 0M, 3.5M and 8M urea.

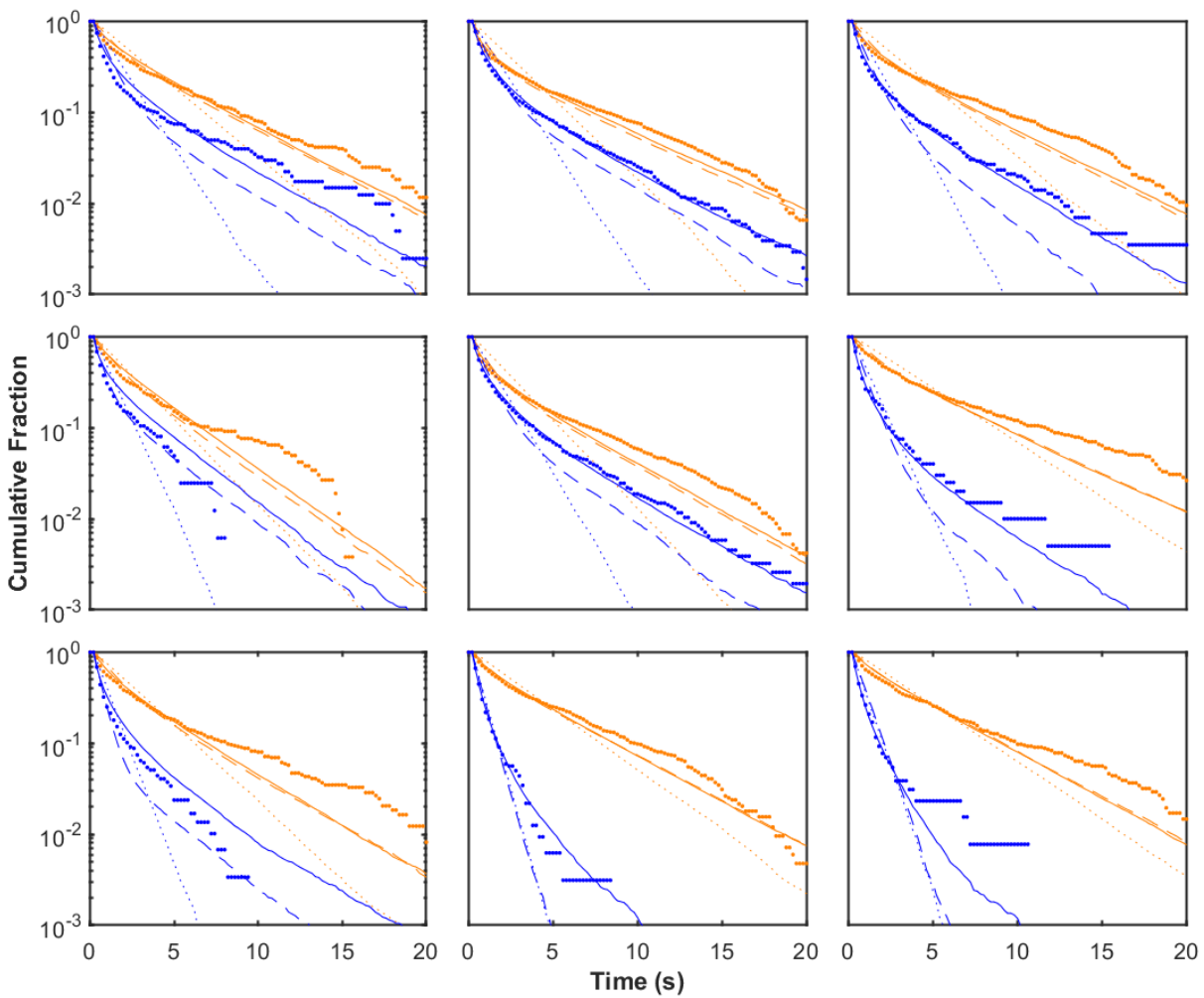


Figure S6 Semi-log plot showing the complimentary cumulative state dwell-time distribution (circles) for folded (blue) and unfolded (orange) NfsB. The system was fit assuming a single population with homogeneous folding and unfolding kinetics (dotted line), two discrete populations with distinct kinetics (dashed line) and continuously variable kinetic parameters (solid lines). From left to right, the plot correspond to physically adsorbed, nonspecifically tethered and site-specifically tethered NfsB, while from top to bottom the figure correspond to 0M, 3.5M and 8M urea.

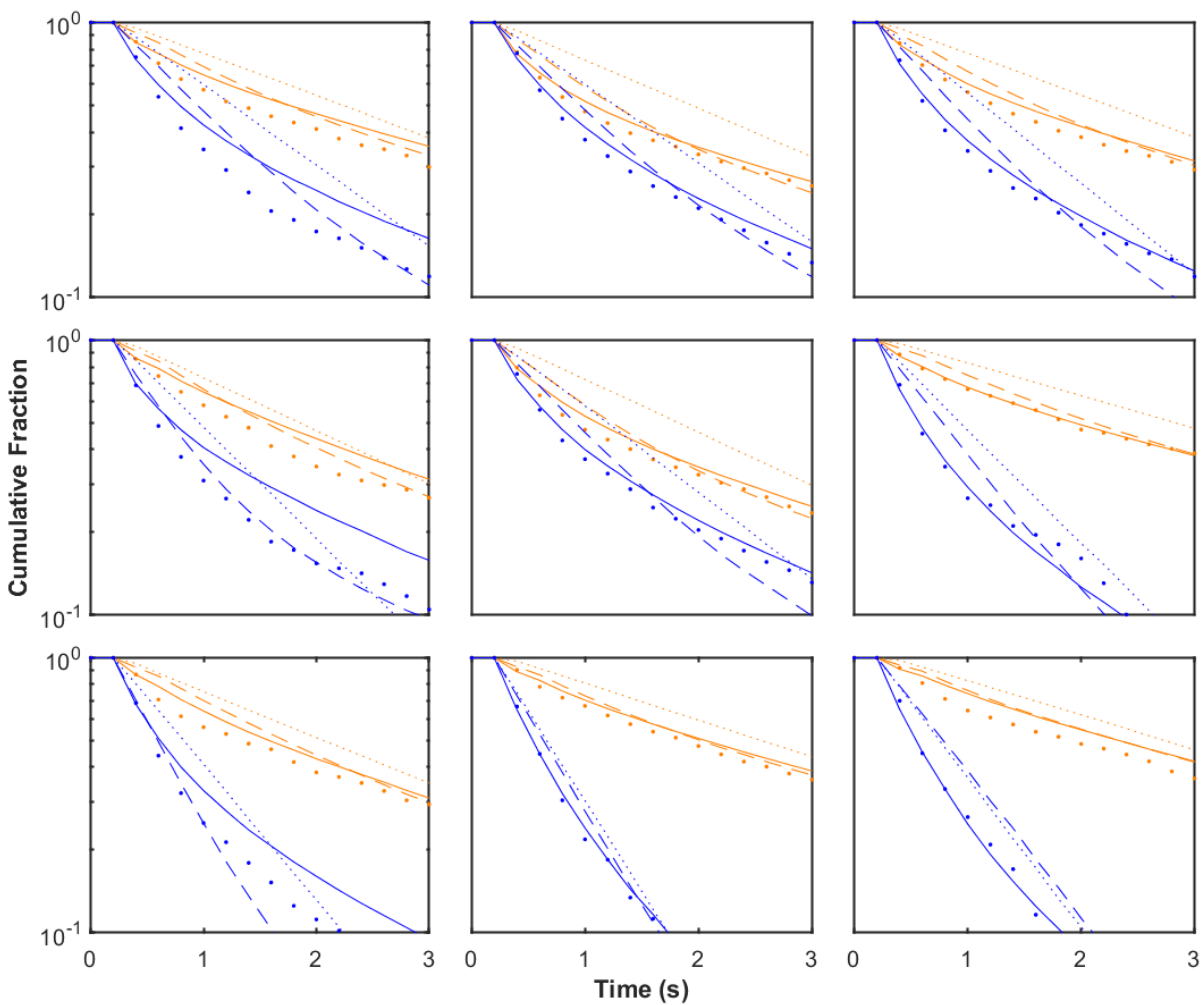


Figure S7 Plots of the same data shown in Figure S8 except that it is zoomed in to show more detail at low dwell times, where the model with continuously variable kinetic parameters is typically superior to the other 2 models. From left to right, the plot correspond to physically adsorbed, nonspecifically tethered and site-specifically tethered NfsB, while from top to bottom the figure correspond to 0M, 3.5M and 8M urea.

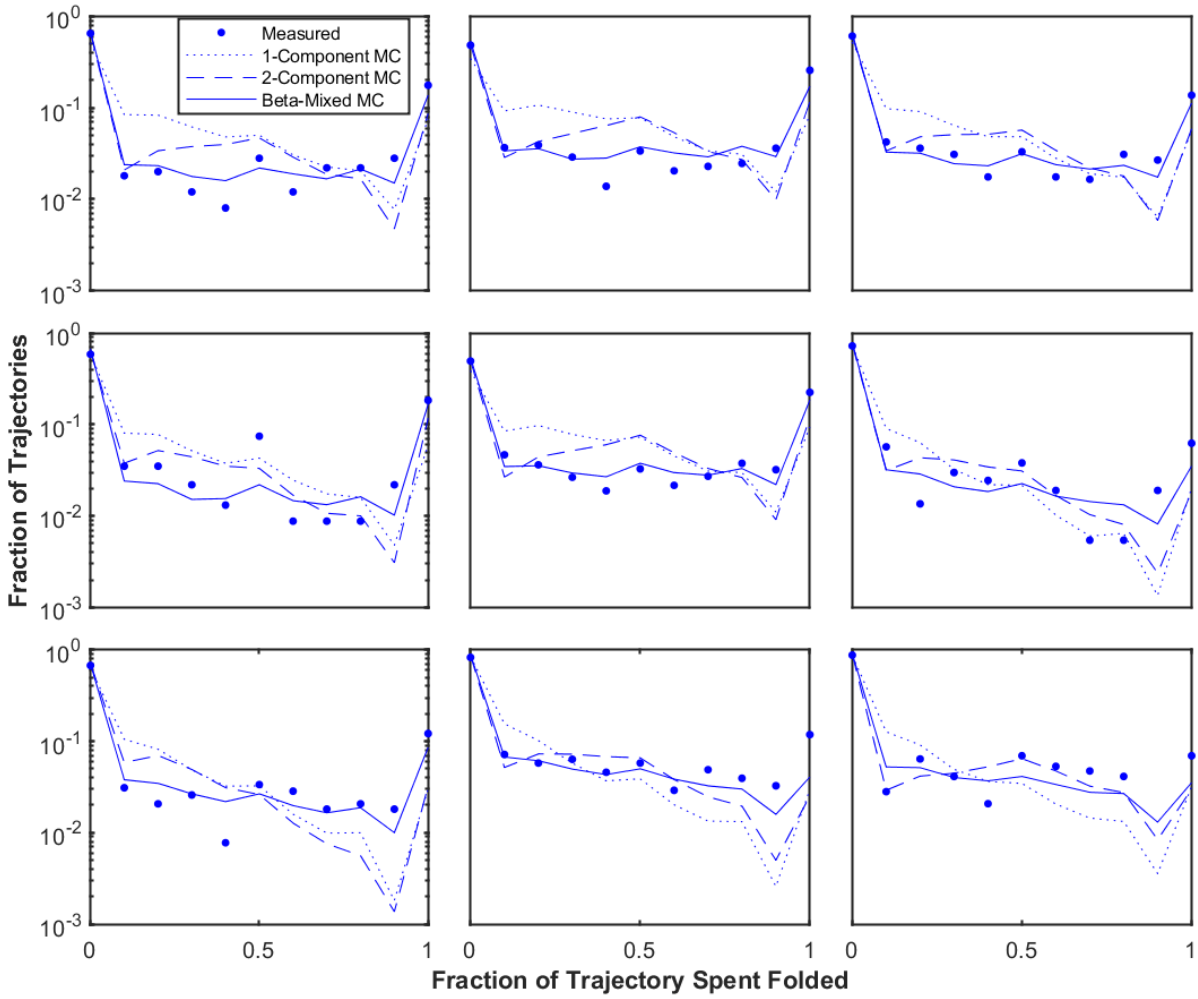


Figure S8 Semi-log plot showing the distribution of the fractions of time that each trajectory spent in the folded state (circles). The system was fit assuming a single population with homogeneous folding and unfolding kinetics (dotted line), two discrete populations with distinct kinetics (dashed line) and continuously variable kinetic parameters (solid lines), where MC stands for Markov chain. From left to right, the plot correspond to physically adsorbed, nonspecifically tethered and site-specifically tethered NfsB, while from top to bottom the figures correspond to 0M, 3.5M and 8M urea.

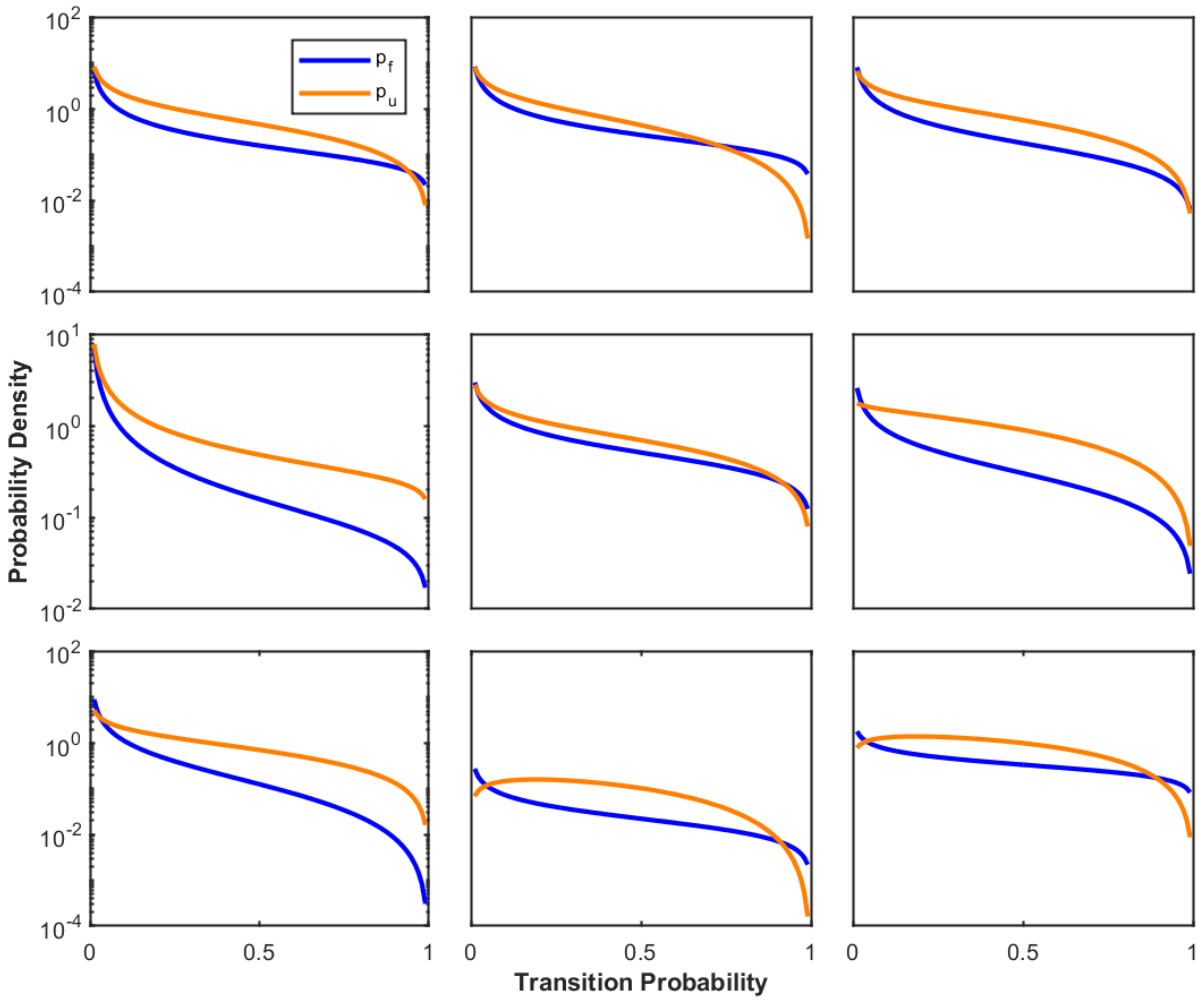


Figure S9 Plots showing the beta distributions of folding and unfolding transition probabilities corresponding to the best-fit beta-mixed Markov-Chain model shown by the solid lines in Figures S8-S10. From left to right, the plot correspond to physically adsorbed, nonspecifically tethered and site-specifically tethered NfsB, while from top to bottom the figures correspond to 0M, 3.5M and 8M urea.

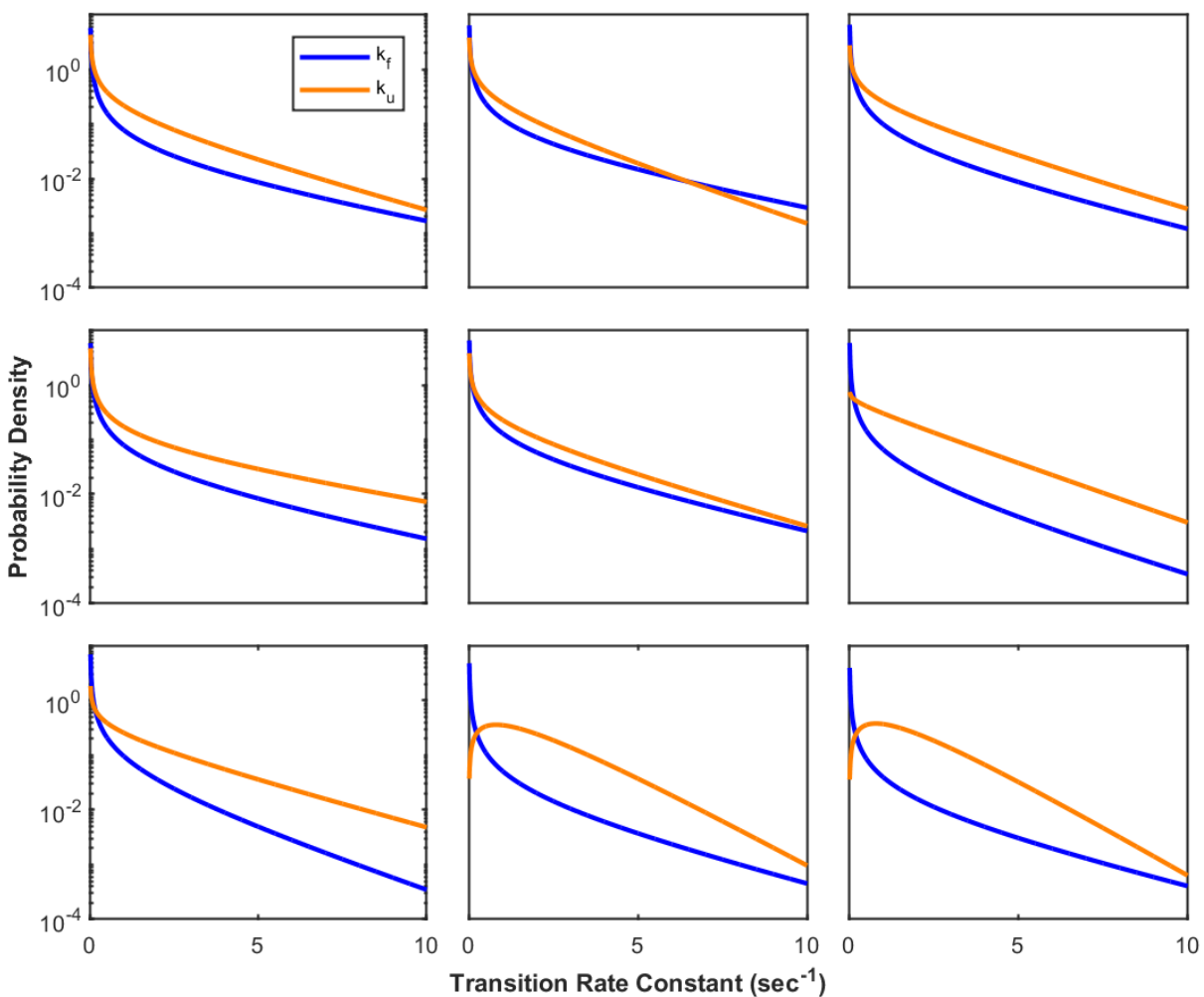


Figure S10 Plots showing the probability density of the folding and unfolding rate constants corresponding to the best-fit beta-mixed Markov-Chain model shown by the solid lines in Figures S8-S10, and corresponding to the distributions of transition probabilities shown in Figure S11. From left to right, the plot correspond to physically adsorbed, nonspecifically tethered and site-specifically tethered NfsB, while from top to bottom the figures correspond to 0M, 3.5M and 8M urea.

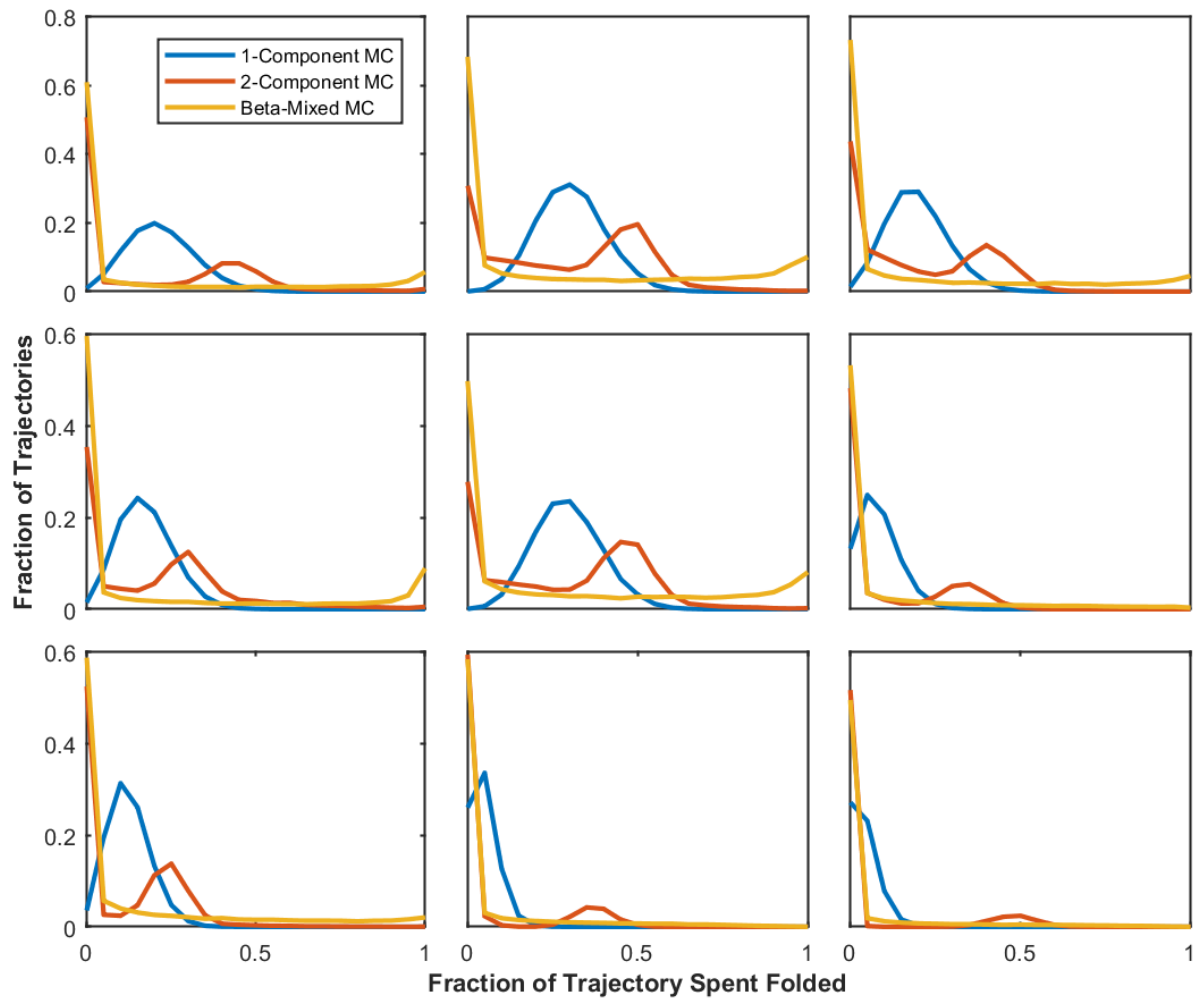


Figure S11 P_{fold} distribution simulated using each of the 3 models used to describe the enzyme conformational dynamics. The simulations are described in section 4. From left to right, the plot correspond to physically adsorbed, nonspecifically tethered and site-specifically tethered NfsB, while from top to bottom the figures correspond to 0M, 3.5M and 8M urea.

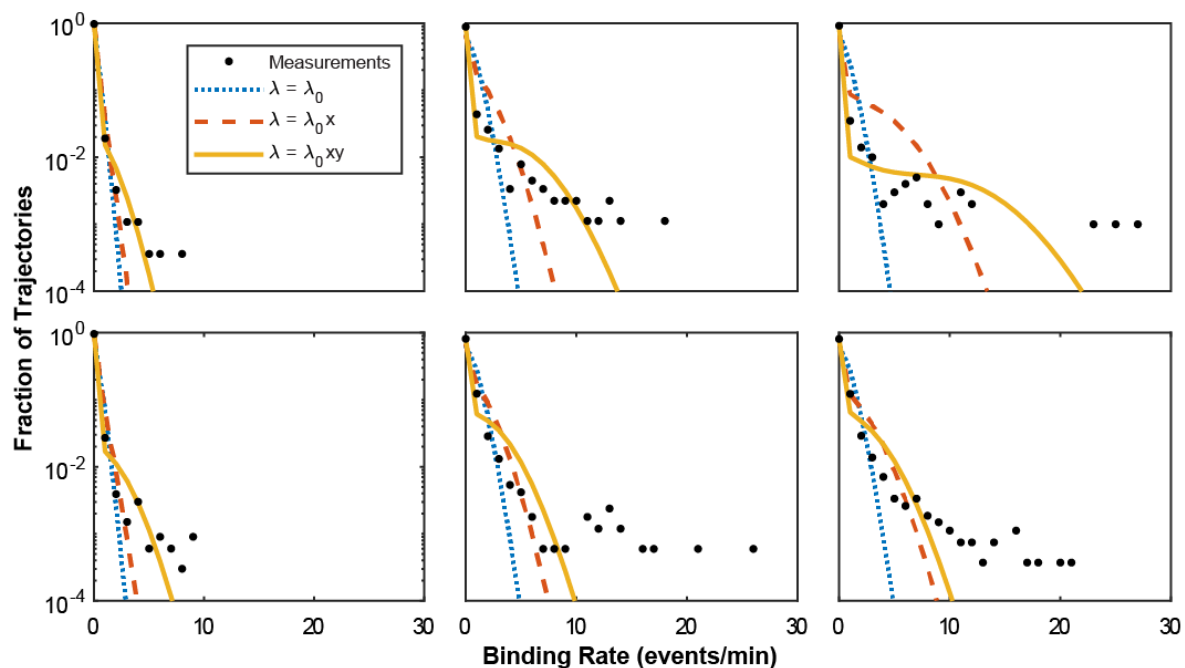


Figure S12 Semi-log plot showing the measured binding rate distribution of FMN (top row) and LF (bottom row) on NfsB immobilized by physical adsorption (left) non-specific tethering (middle) and specific tethering (right) along with the best fit distributions when modeled using a single Poisson distribution ($\lambda = \lambda_0$) and two Poisson mixture models; one which accounts for the fraction of time spent folded, x , and one which accounts for both x and additional loss of activity for reasons other than the folding state, y .

9. References

1. Faulón Marruecos, D.; Kienle, D. F.; Kaar, J. L.; Schwartz, D. K., Grafting Density Impacts Local Nanoscale Hydrophobicity in Poly(Ethylene Glycol) Brushes. *ACS Macro Letters* **2018**, 498-503.
2. Chaparro Sosa, A. F.; Kienle, D. F.; Falatach, R. M.; Flanagan, J.; Kaar, J. L.; Schwartz, D. K., Stabilization of Immobilized Enzymes via the Chaperone-Like Activity of Mixed Lipid Bilayers. *ACS Appl. Mater. Interfaces* **2018**, *10*, 19504-19513.